

Large-scale Rossby wave and synoptic-scale dynamic analyses of the unusually late 2016 heatwave over Europe

Philipp Zschenderlein¹,
Georgios Fragkoulidis²,
Andreas H. Fink¹ and
Volkmar Wirth²

¹Institute of Meteorology and Climate
Research, Karlsruhe Institute of
Technology, Germany

²Institute of Atmospheric Physics,
Johannes Gutenberg University, Mainz,
Germany

Introduction

Among the robust statements in the 5th IPCC (Intergovernmental Panel on Climate Change) report was the assertion that heatwaves in Europe will be more frequent and intense at the end of the twenty-first century (Collins *et al.*, 2013). Observations show an accelerated increase in mean surface temperatures over Europe since the middle of the twentieth century, and observational studies hint at an already elevated probability of heatwaves in this region (Hartmann *et al.*, 2013). Notable recent heatwaves struck western Europe and Russia in summer in 2003 and 2010, respectively, and had large socio-economic impacts (Fink *et al.*, 2004; Russo *et al.*, 2015; Quandt *et al.*, 2017). There is a diversity of studies on the subject of heatwaves and the role of soil moisture anomalies on seasonal and climate timescales (e.g. Fischer *et al.*, 2007), but fewer studies have investigated the dynamical development and predictability of heatwaves (e.g. Black *et al.*, 2004; Miralles *et al.*, 2014; Bieli *et al.*, 2015; Quandt *et al.*, 2017). Heatwaves are often associated with the development of ridging or blocking in the upper-level flow, several days prior to the events, which can be related to Rossby wave dynamics (e.g. Fink *et al.*, 2004; Pfahl and Wernli, 2012; Fragkoulidis *et al.*, 2018). Without these large-scale precursors, a heatwave is unlikely to occur, even in the presence of already-desiccated expanses of soil. Under similar large-scale ridging characteristics persisting for 1–3 days prior to peak temperatures, synoptic and mesoscale boundary

layer processes will be more important in determining the exact value of the maximum temperature at a weather station. This study seeks to shed light on both the large-scale Rossby wave behaviour and the

local processes that contributed to the three peaks of the heatwave that affected southwestern, western and central Europe in late summer and early autumn 2016. The role of the local processes – that is, horizontal

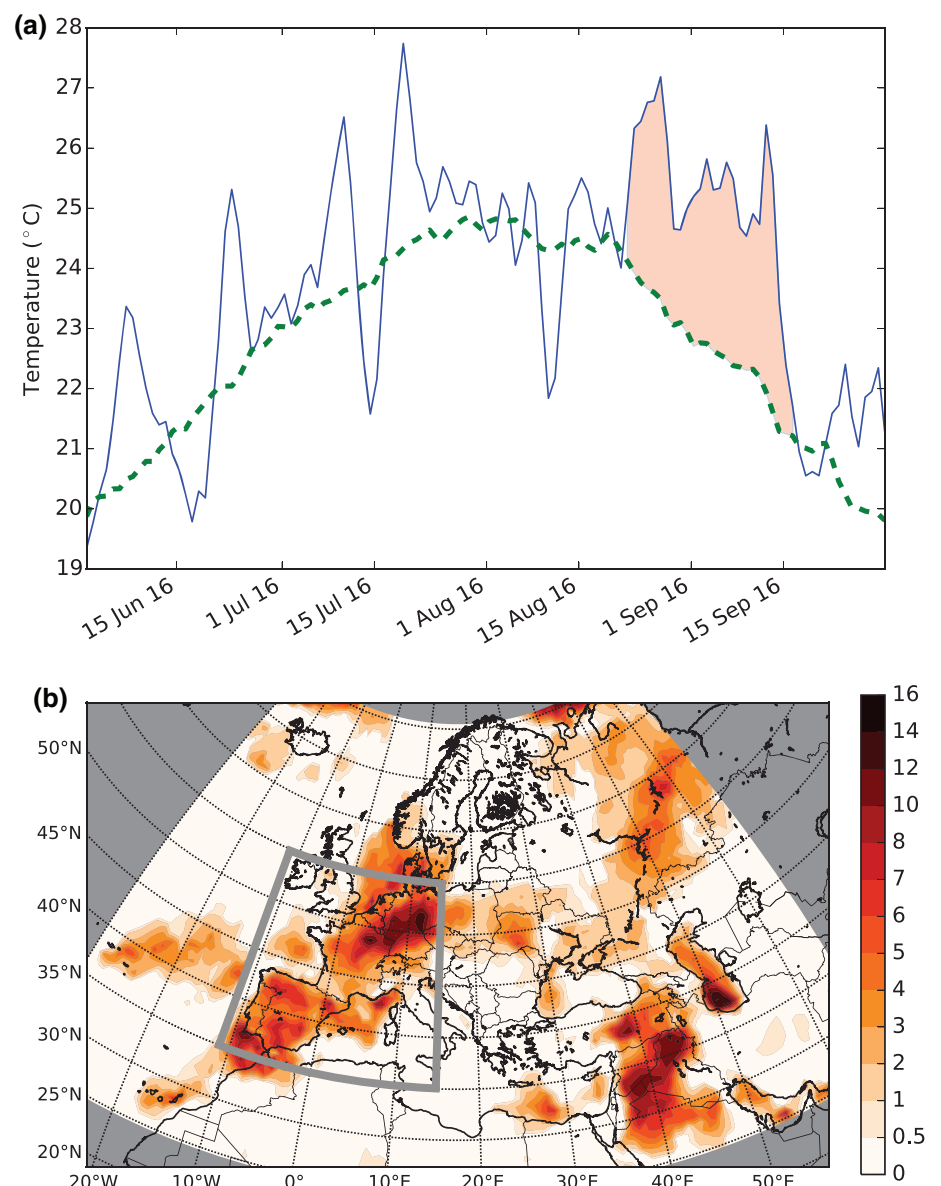


Figure 1. Spatio-temporal extent of the late summer heatwave in 2016. (a) Time series of area-averaged (35°–55°N, 11°W–15°E; see rectangle in panel (b)) daily maximum 2m temperature between 1 June and 30 September 2016. The green dashed line shows the daily ERA-Interim climatology for the reference period 1979–2016. The red filled area corresponds to the heatwave from 23 August to 16 September 2016. (b) Accumulated Heatwave Magnitude Index daily (HWMId, Russo *et al.*, 2015) values for the heatwave period.

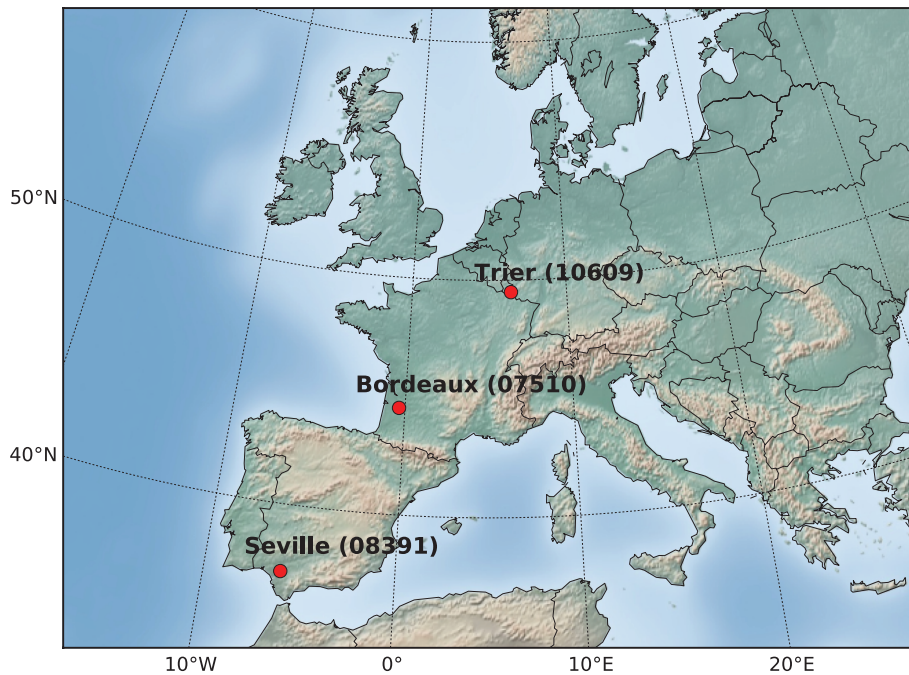


Figure 2. Map showing the locations of the weather stations under study: Bordeaux (France), Seville (Spain) and Trier (Germany). Their WMO station numbers are included, in parentheses.

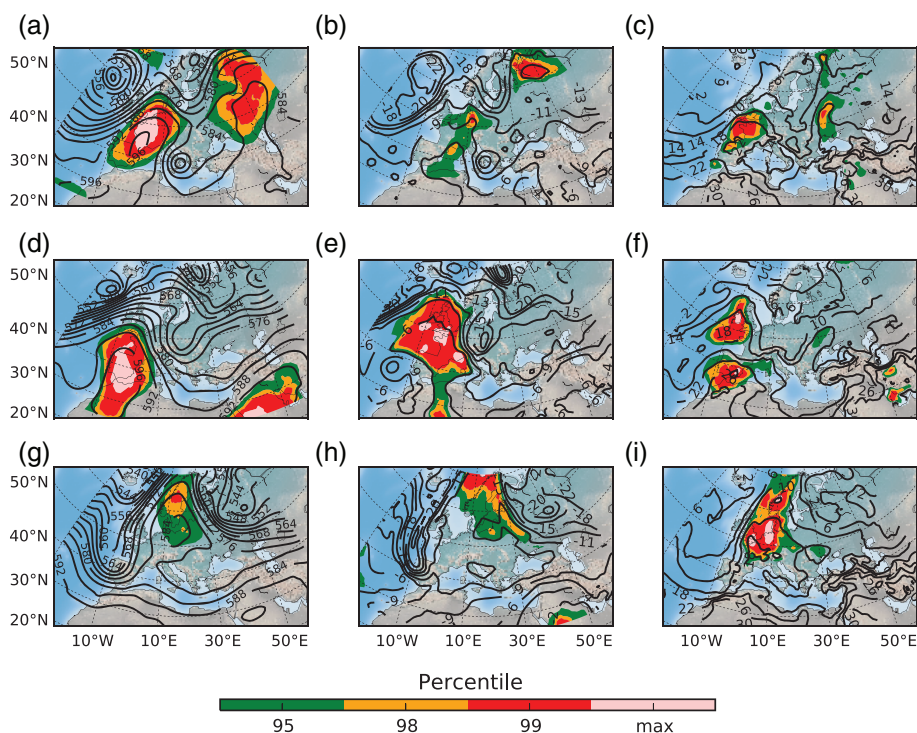


Figure 3. Synoptic overview for the three peaks during the heatwave, on (a, b, c) 23 August 2016, (d, e, f) 5 September 2016, and (g, h, i) 13 September 2016. The column of three plots on the left-hand side (a, d, g) shows geopotential height at 500hPa in gpdam; the middle column (b, e, h) shows temperature at 500hPa in °C, and the right-hand column shows temperature at 850hPa in °C. These variables are contoured, and the areas for which values exceed the 95th, 98th and 99th percentiles – and the highest value recorded for the reference period 1979–2016 – are colour-shaded (see label bar).

temperature advection, adiabatic compression by subsidence, and heat fluxes – will be investigated. These are all terms of the Eulerian form of the temperature tendency equation (Carlson, 1994). The path of the Rossby wave packets can be traced back over the Atlantic using a diagnostic technique proposed by Fragkoulidis *et al.* (2018).

The 2016 late-summer heatwave is remarkable in that it set the stage for the development of the first-ever reported tropical-like storm in the Bay of Biscay (Maier-Gerber *et al.*, 2017). These authors noted the record-breaking sea surface temperatures (SSTs) in the Bay of Biscay, which were consequences of the calm, sunny, warm weather

in the weeks leading up to the ‘Biscane’ (named as a counterpart to the ‘Medicane’ – a Mediterranean hurricane) *Stephanie* on 15 September 2016. Figure 1(a) shows the ERA-Interim-based time series (cf. Dee *et al.*, 2011) of daily maximum 2m temperature, averaged between 35°–55°N and 11°W–15°E (the region bounded by the rectangle in Figure 1(b)) for June to September 2016, in comparison with the daily climatology for 1979–2016. The summer of 2016 was characterised by several short warm periods, especially in June and July. Towards the end of the summer season, a heatwave commenced around 23 August and lasted until mid-September. With three peaks occurring around 23 August, 5 September and 13 September, mid-summer temperature levels persisted throughout a period over which the climatological temperature exhibits a large decrease (green dashed line in Figure 1(a)). As a consequence, the temperature anomalies steadily increased. Based on a commonly used, temperature-based heatwave index, which is discussed in the next section, the largest positive temperature anomalies were observed in Spain and central and western Europe (Figure 1(b)). Bordeaux, in southwestern France, registered a maximum daily temperature of 37°C during the first peak on 23 August 2016. The second peak was record-breaking, in particular for southern Spain. Seville measured 44.8°C, which was the highest temperature on record for any September month at this station. The last peak mainly affected central Europe, where, for example, Trier measured 34.2°C on 13 September 2016, which was also the highest temperature on record for any day in September at this station. The locations of the three stations are shown in Figure 2. In the following sections of this article we will examine the magnitude of the heatwave, its evolution in the upper troposphere, and the relative roles of temperature advection, subsidence and boundary layer heat fluxes, with the aim of explaining the occurrence of the temperature extremes at the three aforementioned European cities.

Magnitude of the heatwave

In order to quantify the onset, termination, and magnitude of the heatwave, we used the percentile-based heat index (Heat Wave Magnitude Index daily, HWMI_{daily}) after Russo *et al.* (2015). According to their definition, a heatwave is a period of at least three consecutive days for which the daily maximum temperature exceeds the 90th percentile of a 31-day period centred on this day. The magnitude of the heatwave is then determined in two steps. First, the difference between the daily maximum temperature and the 75th percentile of the annual maximum temperatures, normalised by the interquartile range,

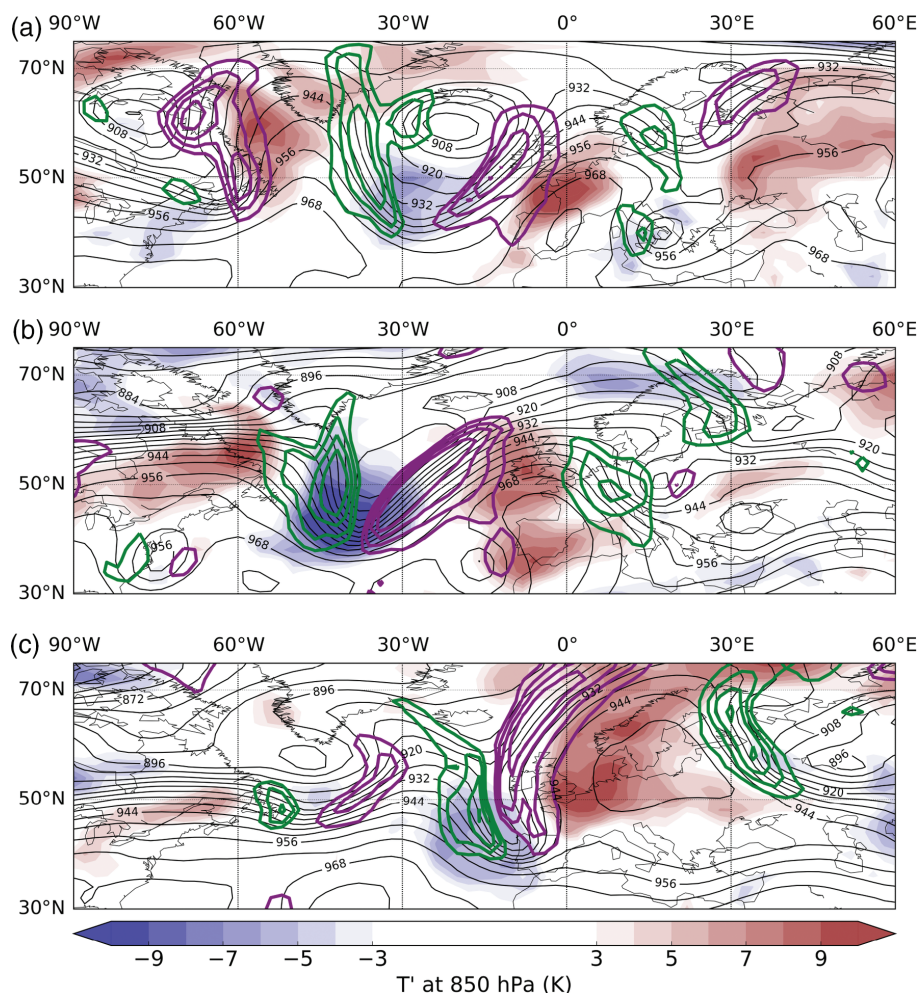


Figure 4. Relationship between 300hPa waviness and low-level temperature anomalies for the three peaks of the heatwave. Geopotential height (black contours, in gpdam) and meridional wind isotachs (with contours, northerlies in green, and southerlies in purple) starting at 20ms^{-1} , then every 10ms^{-1} . Coloured areas denote temperature anomalies at 850hPa (reference period 1979–2016). (a) 23 August 2016, (b) 5 September 2016, and (c) 13 September 2016.

is calculated for each heatwave day. These values are then summed up over the whole heatwave period at each grid point, giving its HWMI value (Figure 1(b)). In view of the decrease of the climatological temperature towards the end of August and during September (Figure 1(a)), we had to adjust the reference period used to calculate the heat index. More specifically, as a climatological reference we only considered annual maximum temperatures between 15 August and 30 September 1981–2010. Figure 1(b) shows the HWMI sum for 2m temperatures for the heatwave period 23 August–16 September. Contrary to the methods of Russo *et al.* (2015), the index was calculated over both land and ocean – positive values above land surfaces indicate high surface temperatures, whereas positive values above the oceans indicate high SSTs, due to their strong influence on 2m temperatures. Central and western Europe were particularly affected during the first and last peaks, whereas the second peak was very intense for Spain, thus resulting in the cumulative heat index displayed in Figure 1(b). Adjacent waters also showed

high HWMI values, especially over parts of the Bay of Biscay, the Gulf of Cadiz and the Gulf of Lion, and the North and Baltic Seas. Note that in the North Sea, for the first time since observations began in 1968, the highest SSTs were recorded in September rather than August (BSH, 2016). Compared with the 2003 heatwave mentioned in the Introduction, the spatial extent of the 2016 heatwave was comparable, but the HWMI values were smaller for 2016 (not shown). It should be noted that this could be due to differences in both the magnitudes and the durations of the heatwaves.

The HWMI index can also be applied to the data for the temperature at 850hPa (not shown). While a similar overall spatial pattern emerged, higher values at 850hPa occurred over the UK and the North Sea, suggesting that the maritime climate of the British Isles diminished the warmth at the surface.

Synoptic evolution

In this section, the spatio-temporal evolution of the heatwave is examined from a

synoptic perspective. The first peak of the heatwave on 23 August 2016 was associated with an extremely strong 500hPa ridge that extended from the Iberian Peninsula across central Europe to the southern parts of Scandinavia. The maximum geopotential height value of approximately 596gpdam was located near the Pyrenees. As can be inferred from the pink shading in Figure 3(a), the highest geopotential height values for the 1979–2016 period were recorded over large parts of west and southwest Europe on this day. The percentile values given for any particular day in Figure 3 were calculated with respect to a centred 21-day window (for 1200 UTC only), spanning the years 1979–2016. Eastern France recorded the highest geopotential height since 1979. Though they were not as extreme as the geopotential height measurements, temperatures at 500hPa (Figure 3(b)) were also very high, with values above the 95th percentile covering much of western Europe. At the western flank of the ridge, extremely high temperatures dominated at 850hPa (Figure 3(c)), with values exceeding 22°C over France. At this time of year, such high temperatures are very unusual poleward of 40°N in western Europe and correspond to the top 1% of the climatological distribution (red areas in Figure 3(c)). The upper-level ridge propagated eastwards over the following few days, after which the flow became more zonal and the heatwave weakened. The second peak of the late summer warmth primarily affected Spain and evolved under a strong ridge extending over southwestern Europe. Similar to the first peak, a large area surpassed the highest geopotential height values on record (Figure 3(d)), with a maximum of 599gpdam measured in southern Spain. However, this time the region of highest geopotential heights was displaced to the southwest and was located over Spain and northern Morocco. In contrast to the first peak, temperatures at both 500 and 850hPa reached record values (Figures 3(e) and (f)), though the areas were not as large and contiguous as their geopotential height equivalents. Small areas of record-breaking temperatures at 850hPa were observed over Ireland and southeastern Spain, with absolute values of 17°C and 26°C , respectively. As a consequence, the thermal tropopause, according to measurements derived from sounding data from Murcia, Spain, reached altitudes of about 15km (not shown) – values which are in keeping with observations of tropical air masses. The final peak of the heatwave was related to an ‘Omega-type’ blocking, with the ridge centred over central Europe and Scandinavia. The ridge pattern for the preceding days was similar, leading to the interruption of the prevailing westerlies over central Europe and providing conditions that were conducive to the occurrence of extreme temperature events

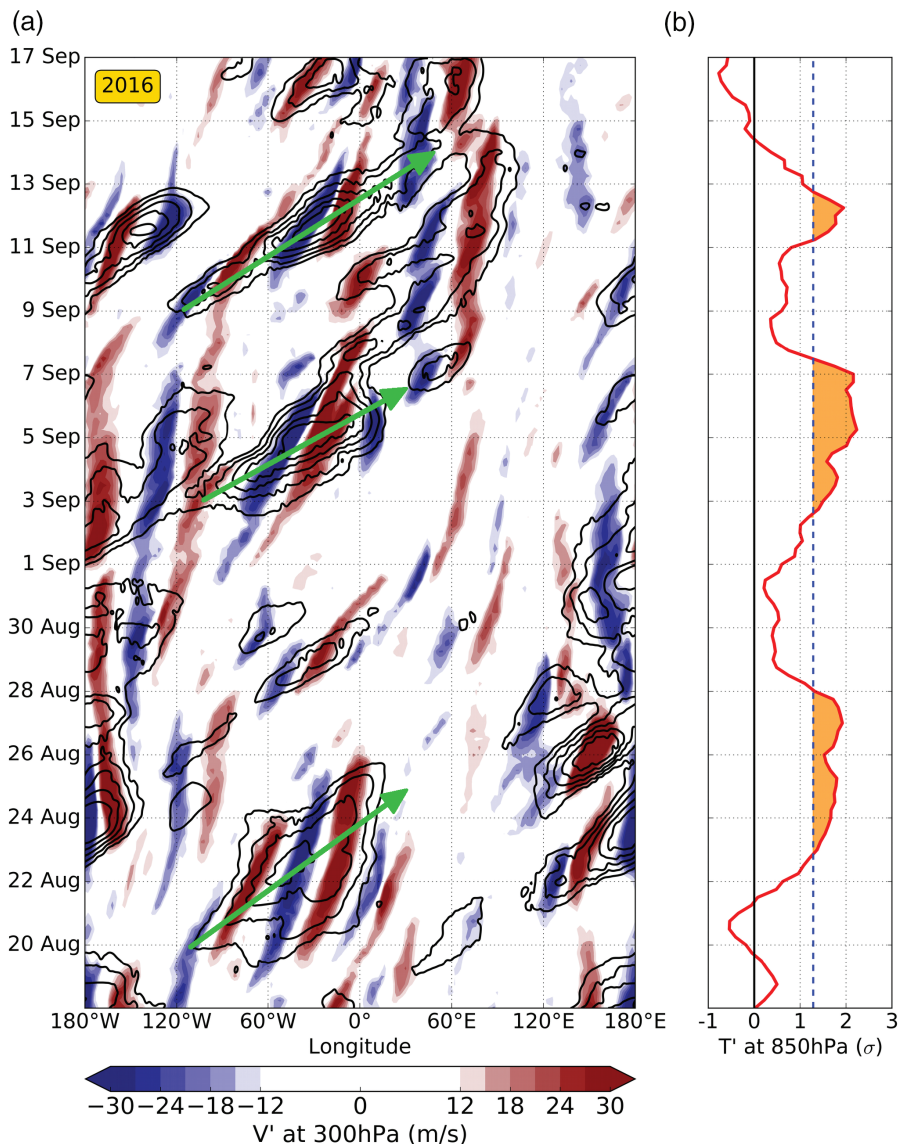


Figure 5. Hovmoeller diagram illustrating the upper tropospheric dynamics for the 2016 heatwave. The contours in (a) depict 300hPa RWP amplitude (in ms^{-1} ; contours every 4ms^{-1} from 22 to 38ms^{-1}). A weak bivariate interpolation (using cubic Hermite splines) has been applied to slightly smoothen the resulting field. The colour fill represents the 300hPa meridional wind anomaly (blue for northerlies and red for southerlies). The time resolution is 6h. Both fields were averaged over a 20° latitude band which self-adjusts (within the 30°N – 70°N band) to those latitudes in which the highest RWP amplitudes occur. The green arrows represent the approximate group velocity of the eastward-propagating RWPs. (b) Normalised temperature anomaly at 850hPa (red line) averaged over 35° – 55°N and 11°W – 15°E (with a $\cos(\text{latitude})$ weighting). Orange shading corresponds to temperature anomaly values in excess of the 90th percentile for the months of August and September (blue dashed line).

(Pfahl and Wernli, 2012). While 500hPa geopotential height and temperature values on 13 September 2016 were by far less extreme than during the previous two heat peaks (Figures 3(g) and (h)), the 850hPa temperatures were extreme under the western flank of the ridge over northwestern Europe and Scandinavia, with values over the English Channel and North Sea (above 18°C) being the highest in the reference period (Figure 3(i)). Finally, it is worth noting that the elongated trough extending down to the western Iberian Peninsula later developed into a cut-off low over the Bay of Biscay that led to the development of the Biscane *Stephanie* (Maier-Gerber *et al.*, 2017).

Large-scale atmospheric precursors

In this section, we present a large-scale perspective of the heatwave by trying to describe the upstream development of the Rossby wave packets (RWPs) in which the ridges described in the previous section were embedded. A large-amplitude RWP can be considered as the envelope encompassing a series of high-amplitude ridges and troughs in the upper-level flow. The activity of RWPs has been shown to be related to surface weather conditions (Wirth *et al.*, 2018). Figure 4 shows maps of anomalous meridional wind v' (the prime

denoting anomalies from the de-trended 1979–2016 mean; see Fragkoulidis *et al.* (2018) for details) at 300hPa, temperature T' at 850hPa and geopotential height at 300hPa for the three days corresponding to the three peaks in Figure 1(a). In all cases, waviness at 300hPa over the North Atlantic/Europe region was apparently high. Deep 300hPa troughs upstream of Europe were marked by strong southerly winds at their eastern flanks, with the 850hPa temperature anomalies being located farther downstream of the wind maxima (Figure 4). The time evolution of the RWP can be studied using a refined RWP diagnostic described in Fragkoulidis *et al.* (2018) that allows one to track zonally constrained wave packets propagating eastwards in a self-adjusting latitude band, instead of assessing the Rossby waviness along an entire latitudinal circle using Fourier analysis.

The left panel of Figure 5 shows a circum-global Hovmoeller diagram for the period from mid-August to mid-September 2016, with the 300hPa RWP amplitudes as contours and meridional wind anomalies v' as colour fill. In addition, the right panel of Figure 5 shows the normalised temperature anomalies T' at 850hPa (red line) averaged over 35° – 55°N and 11°W – 15°E , highlighting in orange values in excess of the August–September 90th percentile (blue dashed line). Apparently, three successive periods of extremely high temperatures occurred over Europe between 23 August and 14 September 2016. All of these periods coincided with strong signals of upper-tropospheric waviness, associated with series of strong meridional wind anomalies embedded in the larger-scale RWPs. The meridional wind anomalies mark the troughs and ridges embedded in the RWP. These RWPs formed over western North America (at around 120°W) and propagated eastwards with a group velocity of the order of 30° longitude per day (green arrows in left panel of Figure 5). This is faster than the phase speed of the embedded troughs and ridges that can be inferred from the propagation speed of the meridional wind anomalies. The RWPs acquired their maximum amplitude over the North Atlantic Ocean. Their arrival over Europe concurred with the aforementioned hot periods. Large-amplitude ridges in all three cases provided favourable conditions for the smaller-scale processes that led to warming in the locations under study (see next section). Finally, after the dispersion of the RWPs, the warm air masses were not sustained, and short periods of mild temperatures provided relief to the affected areas.

Figure 5 clearly shows that the enhanced atmospheric upper-level waviness is a mid-latitude propagating phenomenon that can be traced back upstream a few days before the event and is initiated several

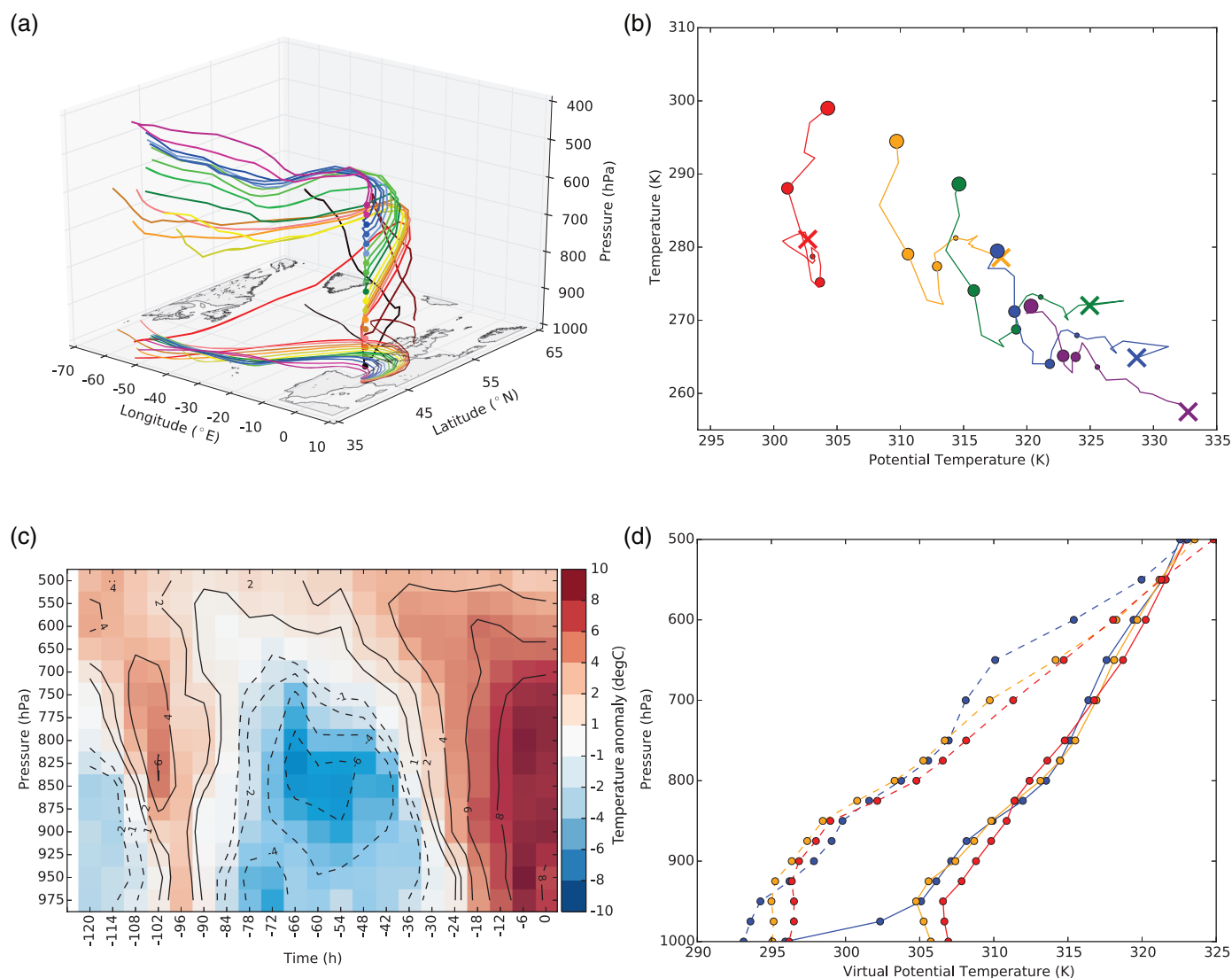


Figure 6. Lagrangian and Eulerian perspectives of the development of the peak of the heatwave in Bordeaux between 1200 UTC on 18 August and 1200 UTC on 23 August 2016. (a) Three-dimensional representation of 5-day backward trajectories, started over Bordeaux between 975 and 550 hPa in 25 hPa increments. Only starting levels at which temperatures exceeded the 95th percentile at 1200 UTC on 23 August 2016 were used. The surface position of the parcel is given on a two-dimensional map (bottom layer), with the colours indicating identical trajectories (black/reddish: 975–900 hPa, orange/yellowish: 875–800 hPa, greenish: 775–700 hPa, blueish: 675–600 hPa, purple: 575–550 hPa). (b) T- Θ diagram (as described in Box 1) showing the evolution of the mean T and Θ values for the trajectories shown in (a), grouped into 5 pressure levels that started over Bordeaux: 975–900 hPa (red), 875–800 hPa (orange), 775–700 hPa (green), 675–600 hPa (blue) and 575–550 hPa (purple). The filled circles of decreasing size represent 24-h intervals prior to 23 August 2016 (i.e. 0, 24, 48 and 72h). The cross indicates the origin. (c) 6-hourly vertical temperature anomalies (degC; base period 1979–2016) over Bordeaux for 18–23 August 2016. (d) Vertical virtual potential temperature profiles Θ_v for 18 August (dashed, pre-heatwave) and 23 August (heatwave) at 0600 (blue), 1200 (orange) and 1800 UTC (red).

thousand or, as for the second heatwave with a potential precursor in the Pacific Ocean, more than 10 000 km to the west of Europe. The related large-scale, sometimes even planetary-scale, Rossby wave dynamics suggest a relatively high degree of predictability – and indeed at lead times of a few days, the data from the 51 members of the ECMWF ensemble prediction system shifted towards positive anomalies for Bordeaux, Seville, and Trier, indicating increasing probabilities of an imminent heatwave at the respective locations (not shown). A similar observation is included in a study by Magnusson *et al.* (2015) for a heatwave affecting Paris, France in July 2015. However, the spatio-temporal details of the extent of the body of warm air ultimately depend on

the phase velocity and amplitudes of the Rossby waves (i.e. the trough ridge systems embedded in the RWP – see discussion in Fragkoulidis *et al.*, 2018 for the 2003 and 2010 European heatwaves), as well as on the related temperature advection, subsidence and heat fluxes in the boundary layer. The role of the latter two processes will be discussed in the next section.

Development of high temperature extremes near the surface

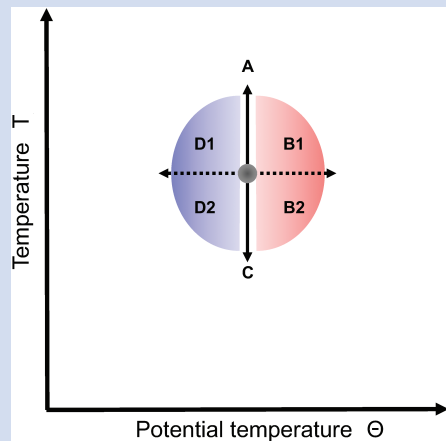
In this section, we will address the following questions: (i) What is the place of origin of the hot air masses? (ii) Which physical processes contribute to the high temperature extremes at the observation

stations? (iii) Does the heat propagate from upper levels to the surface or vice versa? To obtain answers to these questions, we used the Lagrangian trajectory analysis tool developed by Wernli and Davies (1997). We computed 5-day backward trajectories from 6-hourly ERA-Interim wind fields. Trajectories were only started above the three cities if temperatures in the lower and middle tropospheric levels exceeded the 95th percentile of the temperature distribution on 23 August, and 5 and 13 September 2016, respectively.

Figure 6(a) shows 5-day backward trajectories, starting at 1200 UTC on 23 August 2016 between 975 and 550 hPa over Bordeaux (note that trajectories at the surface in this three-dimensional plot are the projection of

Box 1: $T-\Theta$ diagram

The purpose of the $T-\Theta$ phase diagram (Scheme 1) is to distinguish between adiabatic and diabatic temperature changes experienced by an air parcel following its motion (Bieli *et al.*, 2015). The diagram depicts both the temperature T (y-axis) and the potential temperature Θ (x-axis) of an air parcel, and its possible changes. The potential temperature Θ is the temperature that an air parcel would attain when moved adiabatically to 1000hPa. Adiabatic processes are defined as processes that do not change the dry entropy of an air parcel, which implies that the potential temperature is materially conserved following the motion of the parcel and that any changes occur reversibly. Diabatic processes, in contrast, are associated with an exchange of energy between an



Scheme 1. $T-\Theta$ diagram.

air parcel and its environment, resulting in an irreversible material rate of change of the potential temperature. Examples of diabatic processes include radiative processes, subgrid-scale turbulent fluxes (especially in the boundary layer) and the release of latent heat due to phase changes in clouds. When looking at the illustration in Scheme 1, the reader should imagine an air parcel located at the origin of the arrows, as marked by the grey circle. Movements in the strictly vertical direction of the $T-\Theta$ diagram correspond to adiabatic processes, since Θ is conserved. By contrast, diabatic processes occur for all non-strictly-vertical displacements of the parcel in the $T-\Theta$ diagram, with the red (blue) semicircles indicating diabatic heating (diabatic cooling). The parcel may undergo the following changes: increasing T due to subsidence (compression of the air parcel, adiabatic warming), as indicated by the arrow pointing upwards towards the letter 'A'; decreasing T due to lifting (expansion of the air parcel, adiabatic cooling), as indicated by the arrow pointing downwards towards 'C'; increasing Θ due to diabatic warming, but simultaneously decreasing T , which can only be explained by lifting and, hence, adiabatic cooling exceeding diabatic heating (quadrant 'B2'); decreasing Θ due to diabatic cooling, but simultaneously increasing T , which can only be explained by subsidence and, hence, adiabatic warming exceeding diabatic cooling (quadrant 'D1'); the quadrants 'B1' and 'D2' are associated with diabatic heating and cooling, respectively, but no conclusion can be drawn regarding the vertical motion.

the upper-air trajectories, both of which are shown in the same colour). Almost all trajectories arriving at Bordeaux on 23 August 2016 crossed the North Atlantic Ocean between 800 and 500hPa (i.e. above the marine boundary layer). Near Europe, 48h before the event, the air parcels strongly descended along an anticyclonic trajectory to approach Bordeaux from the northeast – that is, the direction from which they travelled for a long time over land – experiencing clear-sky conditions (not shown). The $T-\Theta$ phase diagram (Figure 6(b)), see Box 1 for explanation) clearly illustrates that the air parcels, especially when arriving at lower levels over Bordeaux, experienced a substantial increase in temperature of 20–25 degC due to adiabatic compression 48h prior to the event. The temperature increase is close to adiabatic, as indicated by the very small rate of change of the parcels' potential temperature during this stage (Figure 6(b)). Apparently, this adiabatic warming is consistent with the subsidence visible in Figure 6(a). Just before the extreme temper-

ature event, the trajectories closest to the surface experienced slight diabatic warming (red line in Figure 6(b)), presumably due to turbulent heat fluxes as they were transported above land surfaces (Figure 6(a)). Figure 6(c) shows the development of temperature anomalies between 18 and 23 August in the lower and mid-troposphere above Bordeaux from an Eulerian perspective. Between 90 and 36h before the peak temperatures were reached at 1200 UTC on 23 August 2016, the atmosphere was comparably cold, especially between 900 and 800hPa. The temperatures increased rapidly before the actual extreme temperature event. Interestingly, the positive temperature anomalies initially occurred at higher levels and subsequently penetrated downwards, 'propagating' from the upper levels to the surface. This propagation is consistent with the subsidence, which was remarkably high in the last 36h prior to the heatwave. Overall, this suggests that subsidence and adiabatic compression are the driving factors in the development of high temperatures at the

surface. Figure 6(d) shows diurnal cycles (0600, 1200, 1800 UTC) of vertical profiles of virtual potential temperature Θ_v for the pre-heatwave on 18 August 2016 (dashed lines) and the heatwave on 23 August 2016 (solid lines). The profiles reveal (i) the strong lower tropospheric warming between 18 and 23 August 2016, (ii) the reasonably constant and shallow depth of the well-mixed (i.e. Θ_v nearly constant with height) boundary layer, and (iii) a strong diurnal cycle on 23 August 2016.

Figure 7 shows the same set of panels as Figure 6, but for the hottest September day on record in Seville (5 September 2016). Backward trajectories are only started up to 700hPa, because at higher altitudes the temperatures were not extreme (see Figure 7(c)). Compared with the Bordeaux episode, the air parcels travelled a much shorter distance during the 5 days preceding the Seville heatwave. Although most of the trajectories had an anticyclonic curvature, the individual origins of the air parcels were diverse. Parcels which ended up near the surface in Seville originated in northern Spain, and those ending up at higher altitudes over Seville had their origins mostly over warm northern Africa – a pathway that was favoured by the large-scale setting to the North (RWP) and realised in connection to a short upper-level trough to the southwest of the Iberian Peninsula (Figure 4(b)). Nearly all trajectories entered the Seville area from the east. Parcels arriving near the surface warmed adiabatically in the last 72h by about 30 degC (Figure 7(b)). They experienced subsidence over a longer time period (3 days) than those over Bordeaux (2 days). Again, this suggests that subsidence contributed significantly to this heatwave event. Interestingly, the air parcels starting between 700 and 775hPa in Seville warmed diabatically 48 to 24h before the event. This took place in the surroundings of the Atlas Mountains (Figure 7(a)), which suggests that turbulent heat fluxes and moist convection in this area played an important role. A more detailed analysis of the diabatic processes (including cloud microphysics) is beyond the scope of this study. Figure 7(c) shows the vertical structure of the atmosphere over Seville from 31 August to 5 September. The markedly different behaviour of this heat event compared to the former case is striking. Distinct positive temperature anomalies developed 48h prior to the extreme temperature episode, with a maximum at the surface and the lower tropospheric layers. Compared with the lower planetary boundary layer heights 5 days before the high temperature event in Seville, the boundary layer deepened during the heat event. This can be inferred from the near-constant vertical profile of Θ_v in Figure 7(d). Black *et al.* (2004) also found elevated planetary boundary

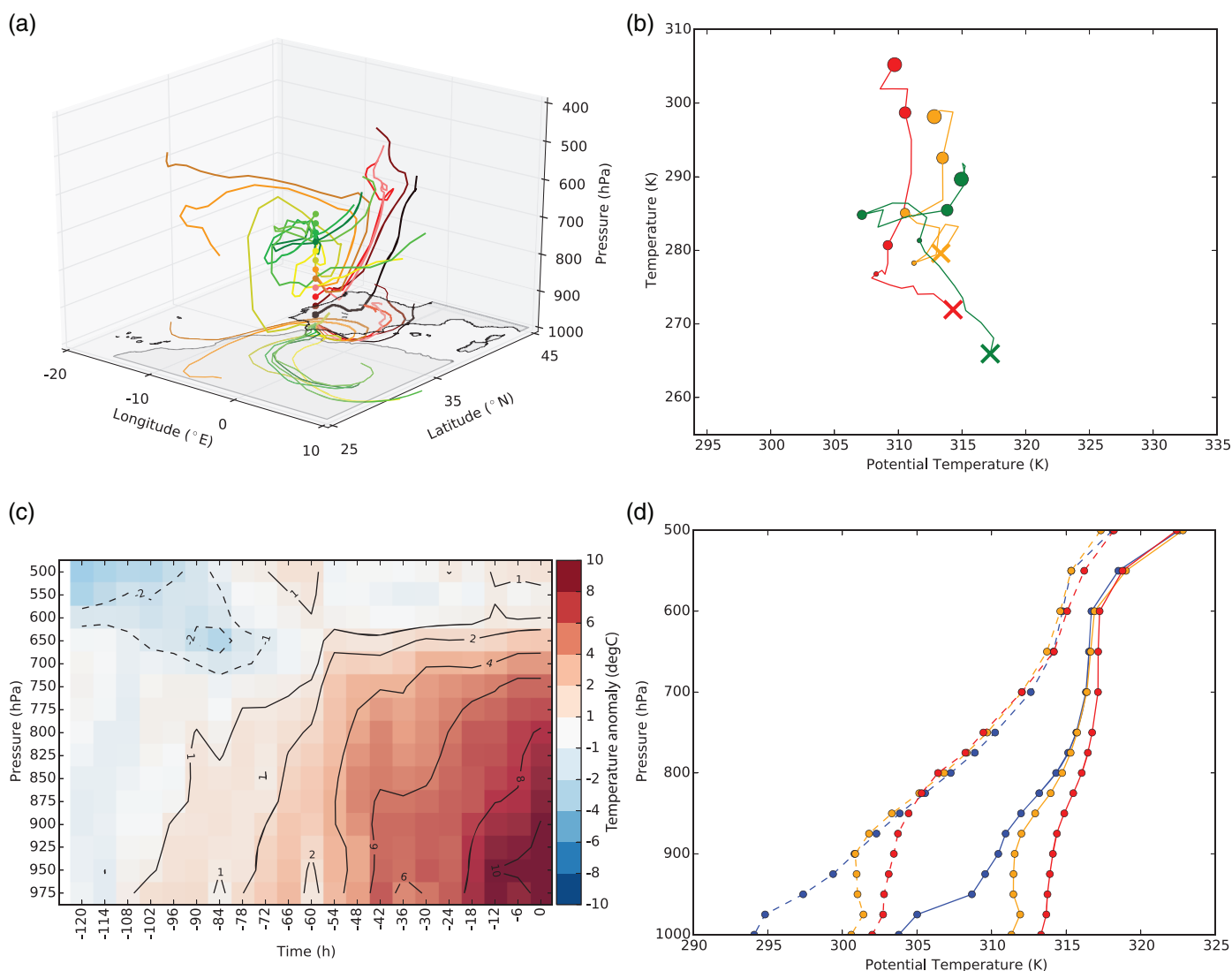


Figure 7. As in Figure 6, but for Seville. Backward trajectories were started between 975 and 700hPa, and the 5-day period under consideration is from 1200 UTC on 31 August to 1200 UTC on 5 September 2016.

layer heights above Paris during the 2003 heatwave. It appears that strong insolation, ensuing surface fluxes and dry convection deepened the boundary layer. The evolution of the temperature profiles suggests a bottom-up development similar to the findings of Miralles *et al.* (2014). Thus, adiabatic compression worked in concert with boundary layer processes to create the hottest September day ever recorded in Seville. Despite the suggested importance of subsidence and boundary layer processes, they cannot be considered to be independent of the RWP. The large ridge embedded in the RWP was instrumental in steering the parcels toward the Seville region on anti-cyclonic trajectories and under clear-sky conditions.

Yet another picture emerged as an explanation of the cause of the hottest September day on record at Trier on 13 September 2016. Most of the trajectories – which started from 975 up to 800hPa, where temperature extremes were present over Trier – originated close to the Rhône valley and northern Italy (Figure 8(a)), yielding a horizontal

transport over comparably short distances and above land surfaces only. The lowest trajectories were trapped in the planetary boundary layer, suggesting significant interaction with the land surface, presumably due to enhanced surface heat fluxes. This can be seen in Figure 8(b) as an increase in potential temperature of approximately 10 deg C (adiabatic heating). The fluctuating temperature shown in Figure 8(b) illustrates the diurnal temperature variation. Note that the diurnal temperature variation is also clearly visible in Figure 8(c), as the lowest temperature anomalies were always attained at 0600 UTC near the surface. The air parcel temperature increases shown in Figure 8(b) are generally smaller than those observed for the other locations, and subsidence from higher levels was not observed for this location. Instead, heat was trapped in the planetary boundary layer and accumulated day by day (Figure 8(c)), leading to an increase in the top of the boundary layer over Trier (Figure 8(d)). The boundary layer top was quite high for this location and time of year (i.e. late in the year). Figure 8(c)

also revealed positive temperature anomalies above Trier up to 500hPa from 8–13 September. We conclude that the main factor in the development of the extreme temperature episode over Trier is the influence of diabatic processes in the planetary boundary layer – for example, heating due to upward-directed surface sensible heat fluxes caused by strong insolation over several days, which was experienced both locally over Trier and by air parcels which reached the region over the same period.

Conclusions

We analysed the planetary- and synoptic-scale developments that led to the 2016 European late summer/early autumn heatwave. Central, western and southwestern Europe were the most affected regions, with record-breaking maximum temperatures in some places. The highest September temperatures since their respective records began were reported at both Seville (44.8 $^{\circ}$ C; records started in 1951) and Trier (34.2 $^{\circ}$ C; records started in 1941). The three peaks

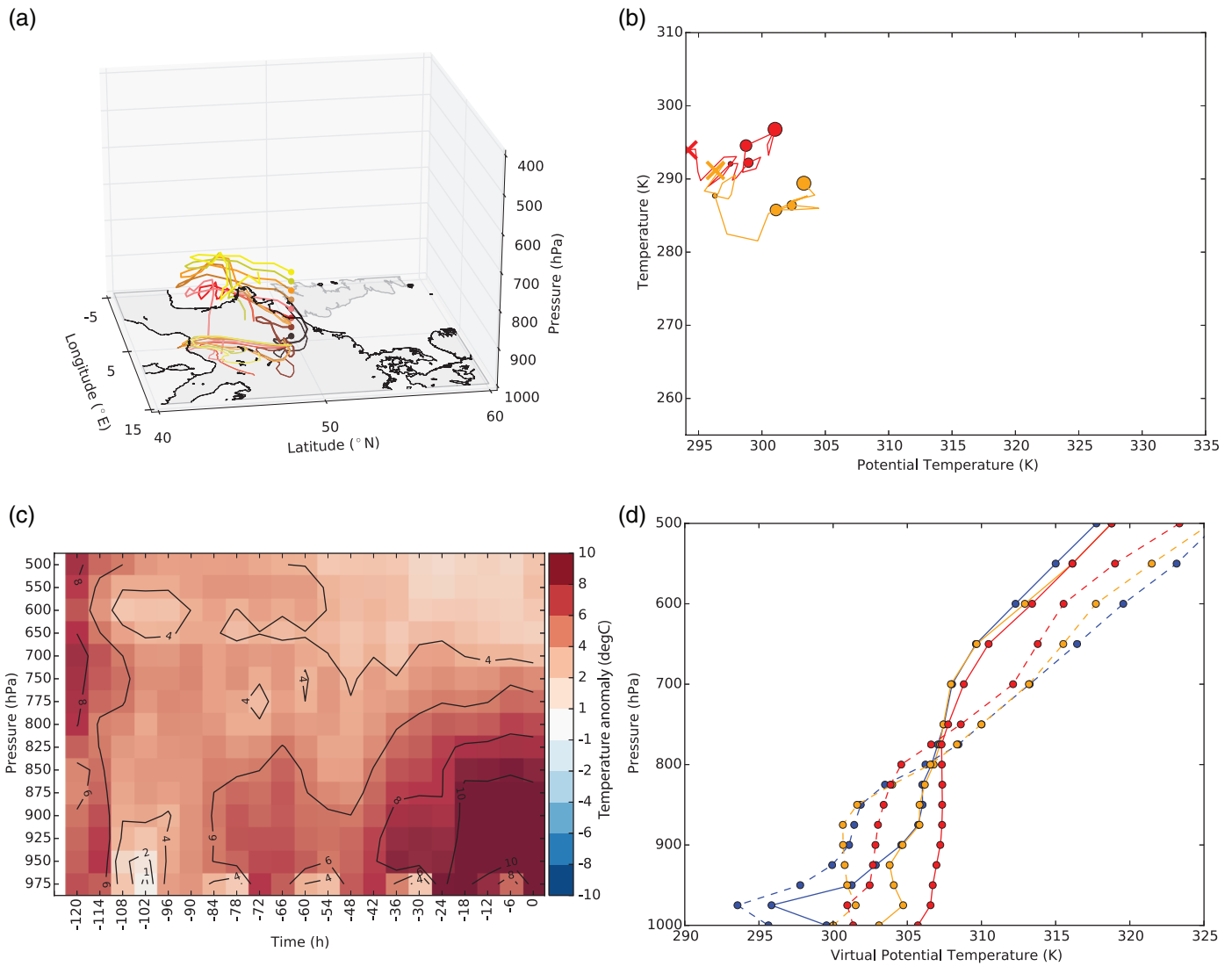


Figure 8. As in Figure 6, but for Trier. Backward trajectories were started between 975 and 800hPa, and the 5-day period considered is from 1200 UTC on 8 September to 1200 UTC on 13 September 2016.

were all accompanied by pronounced 500hPa ridges. The first two peaks showed larger areas with the highest values of geopotential height for that time of the year since at least 1979. The ridges were embedded in eastward-propagating, high-amplitude Rossby wave packets arriving over western Europe. The packets had their origins over western North America. Though it has not been discussed here, it is worth noting that local temperature advection did not play a noticeable role in local temperature changes at Bordeaux, Seville or Trier. On the contrary, the adiabatic compression term due to subsidence exhibited exceptionally high values for the Bordeaux and Seville cases. Changes in the temperatures of subsiding parcels arriving at the lower troposphere at these locations were substantial – of the order of 20–30 degC – in the 2–3 days prior to the peak of the heatwaves. Diabatic processes (such as surface sensible heat fluxes due to enhanced insolation) and dry convection in the boundary layer appeared to be the major explanation for the occurrence of the Trier heatwave event, where hardly any subsidence occurred.

The results presented in this study have potential ramifications for the investigation of the predictability of heatwaves. While dry soils are a prerequisite for heatwaves, an understanding of Rossby wave dynamics may allow for the development of early alerts for imminent heatwave events (cf. Magnusson *et al.* 2015). For the cases discussed in this article, the ECMWF ensemble prediction system indicated an enhanced likelihood of heatwaves up to 5 days in advance (not shown), related to the discussed origin of the Rossby wave packets thousands of kilometres upstream. However, the final magnitude of the heatwave seems to be related to the details of the (thermo-)dynamics associated with the ridge embedded in the Rossby wave packet. The absolute predictability (i.e. whether the observed maximum temperature was well forecast) of the hottest day, at a few days' lead time, was best for Bordeaux, followed by Seville and Trier. However, with respect to the model climatology, the ensemble prediction system showed the highest probabilities for extreme temperatures for Trier first, followed by Seville and Bordeaux (not

shown). The role of the large-scale Rossby wave vs synoptic and mesoscale dynamics for the ensemble predictability of heatwaves at about 1 week to 24h lead times are currently under investigation by the large German weather research initiative 'Waves to Weather' (<http://wavestoweather.de>), which is endorsed by the WMO HIWeather initiative (https://www.wmo.int/pages/prog/arep/wwrp/new/high_impact_weather_project.html). The latter aims at improving resilience to high impact weather by, amongst other approaches, improving probabilistic forecasts. With CMIP6 global and regional climate models having much higher spatial resolution, the large- and synoptic-scale dynamic processes under discussion here can also be meaningfully analysed for heatwaves at the end of the twenty-first century.

Acknowledgements

The research leading to these results has been conducted within the subproject C4: *Coupling of planetary-scale Rossby wave trains to local extremes in heat waves over*

Europe of the Transregional Collaborative Research Center SFB/TRR 165 'Waves to Weather', funded by the German Research Foundation (DFG). We are very thankful to Stephan Pfahl (FU Berlin) and Heini Wernli (ETH Zurich) for inspiring discussions. We also thank two anonymous reviewers and the editor for their valuable comments, which undoubtedly helped to improve the manuscript.

References

- Bieli M, Pfahl S, Wernli H.** 2015. A Lagrangian investigation of hot and cold temperature extremes in Europe. *Q. J. R. Meteorol. Soc.* **141**: 98–108.
- Black E, Blackburn M, Harrison G et al.** 2004. Factors contributing to the 2003 European heatwave. *Weather* **59**: 217–223.
- BSH.** 2016. Press release of the Federal Maritime and Hydrographic Agency of Germany: record warmth left its mark in the North Sea. http://www.bsh.de/de/Das_BSH/Presse/Pressearchive/Pressemitteilungen2016/Pressemitteilung17-2016.pdf (in German; accessed 30 November 2017).
- Carlson TN.** 1994. *Mid-latitude Weather Systems*. Routledge: New York, NY.
- Collins M, Knutti R, Arblaster J et al.** 2013. Long-term climate change: projections, commitments and irreversibility, in *Climate Change 2013: The Physical Science Basis Contribution of Working Group I to the Fifth Assessment Report of the Intergovernmental Panel on Climate Change*. Stocker TF, Qin D, Plattner G-K

et al. (eds), pp. 1029–1136. Cambridge University Press: Cambridge, UK and New York, NY.

- Dee D, Uppala S, Simmons A et al.** 2011. The ERA-Interim reanalysis: configuration and performance of the data assimilation system. *Q. J. R. Meteorol. Soc.* **137**: 553–597.
- Fink AH, Brücher T, Krüger A et al.** 2004. The 2003 European summer heatwaves and drought – synoptic diagnosis and impacts. *Weather* **59**: 209–216.
- Fischer EM, Seneviratne SI, Vidale PL et al.** 2007. Soil moisture-atmosphere interactions during the 2003 European summer heatwave. *J. Clim.* **20**: 5081–5099.
- Fragkoulidis G, Wirth V, Bossmann P et al.** 2018. Linking Northern Hemisphere temperature extremes to Rossby wave packets. *Q. J. R. Meteorol. Soc.* **144**: 553–566.
- Hartmann DL, Klein Tank AMG, Rusticucci M et al.** 2013. Observations: atmosphere and surface, in *Climate Change 2013: The Physical Science Basis. Contribution of Working Group I to the Fifth Assessment Report of the Intergovernmental Panel on Climate Change*. Stocker TF, Qin D, Plattner G-K et al. (eds), pp. 159–254. Cambridge University Press: Cambridge, UK and New York, NY.
- Magnusson L, Thorpe A, Buizza R et al.** 2015. Predicting this year's European heat wave. *ECMWF Newsl.* **145**: 4–5.
- Maier-Gerber M, Pantillon F, Di Muzio E et al.** 2017. Birth of the Biscane. *Weather* **72**: 236–241.
- Miralles DG, Teuling AJ, van Heerwaarden CC et al.** 2014. Mega-heatwave temperatures due to combined soil desiccation and atmospheric heat accumulation. *Nat. Geosci.* **7**: 345–349.

Pfahl S, Wernli H. 2012. Quantifying the relevance of atmospheric blocking for co-located temperature extremes in the Northern Hemisphere on (sub-)daily time scales. *Geophys. Res. Lett.* **39**: L12807. doi:10.1029/2012GL052261

Quandt LA, Keller JH, Martius O et al. 2017. Forecast variability of the blocking system over Russia in summer 2010 and its impact on surface conditions. *Wea. Forecasting* **32**: 61–82.

Russo S, Sillmann J, Fischer EM. 2015. Top ten European heatwaves since 1950 and their occurrence in the coming decades. *Environ. Res. Lett.* **10**: 1–15.

Wernli H, Davies HC. 1997. A Lagrangian-based analysis of extratropical cyclones. I: the method and some applications. *Q. J. R. Meteorol. Soc.* **123**: 467–489.

Wirth V, Riemer M, Chang EKM et al. 2018. Rossby wave packets on the mid-latitude Rossby waveguide – a review. *Mon. Weather Rev.* (in press). doi:10.1175/MWR-D-16-0483.1.

Correspondence to: P. Zschenderlein
philipp.zschenderlein@kit.edu

© 2018 The Authors Weather published by John Wiley & Sons Ltd on behalf of Royal Meteorological Society

This is an open access article under the terms of the Creative Commons Attribution License, which permits use, distribution and reproduction in any medium, provided the original work is properly cited.

doi:10.1002/wea.3278